The use of electrical resistivity tomograms as a parameterization for the hydraulic characterization of a contaminated aquifer

Théo de Clercq, Abderrahim Jardani, Pierre Fischer, Laurent Thanberger, Tan Minh Vu, David Pitaval, Jean-Marie Côme, Philippe Begassat

Udapted 04-16-2020

Research Paper/

The use of electrical resistivity tomograms as a parameterization for the hydraulic characterization of a contaminated aquifer

Théo De Clercq[*1,2], Abderrahim Jardani[1], Pierre Fischer[1], Laurent Thanberger[2], Tan Minh Vu [1], David Pitaval [3], Jean-Marie Côme [3], Philippe Begassat [4]

*Corresponding author

(1) UNIROUEN, UNICEAN, UMR CNRS 6143 M2C Morphodynamique Continentale et Côtière at UFR Sciences et Techniques, Université de Rouen Place Emile Blondel 76130 Mont Saint Aignan, Normandie, France.

(2) VALGO, 2 avenue Gutenberg 31128 Portet sur Garonne, Occitanie, France.

(3) Burgeap GINGER, 143 Avenue de Verdun, 92442 Issy-les-Moulineaux, Ile de France, France.

(4) ADEME, 20 Avenue du Grésillé, 49000 Angers, Pays de la Loire, France.

E-mails : theo.declercq@valgo.com, abderrahim.jardani@univ-rouen.fr; pierre.fischer@univ-rouen.fr; laurent.thannberger@valgo.com; minh-tan.vu@univ-rouen.fr; d.pitaval@groupeginger.com; jm.come@groupeginger.com; philippe.begassat@ademe.com.

Conflict of interest: None.

Key words: electrical resistivity tomogram; hydraulic tomography ; hydrogeophysics ; inversion ; inverse problem ; stochastic inversion.

Article Impact Statement: Use of electrical resistivity data in the hydraulic characterization of a contaminated aquifer by inverting pumping hydraulic data.

Abstract:

Hydraulic characterization of a contaminated aquifer is an important step in depollution processes because its hydraulic parameters control the choice and efficiency of the depollution protocol to be adopted. The characterization presented in this article uses a 3D electrical resistivity imagery to identify the spatial heterogeneities of a contaminated aquifer under tidal influence. Indeed, we use a 3D resistivity model as a source of information to parameterize the reconstruction of the hydraulic conductivity in 3D by inverting a set of hydraulic data acquired on the 13 monitored wells in response to two pumping tests. This parameterization relies on the identification of the main electro-facies in the resistivity model in the saturated zone, which will then be exploited in the hydraulic characterization to find their corresponding hydraulic conductivity values.

This strategy of parameterization permits to reduce the number of the hydraulic conductivity parameters to be identified to eight hydro-facies, with a stochastic algorithm called the Adaptive Metropolis Algorithm. The hydraulic responses associated with the pumping tests are obtained once the natural effect of the tide is removed. The hydraulic conductivity model has permitted to highlight the main heterogeneities in the aquifer in which the hydraulic conductivity is ranging between [$10^{-4.6}$, $10^{-2.8}$ m/s]. This range of variability reveals the permeable and smooth character of the aquifer in which the presence of coarse sand and flint blocks enhances its transmissivity. These permeable zones are electrically identified by resistive anomalies in the 3D electrical resistivity imaging.

Introduction:

The strong industrialization of the last century has led to an increase of contaminated sites that currently represent a real threat to the health of the population and the quality of the ecosystem (air, water, soil, flora and fauna). To address these environmental issues, several remediation technologies have been developed in order to remove contaminants or to reduce their spread in water resources; among them, we cite: natural attenuation, in situ thermal desorption, in situ chemical oxidation or reduction, , hydraulic containment, and pump and treat (Yeung 2010; Zhang et al. 2017; Ossai et al. 2020). However, their applicability and effectiveness still strongly depend on the dynamic of the aquifer, in other terms, to the hydraulic conductivity of soils. The groundwater flow and the migration of contaminant plumes are conditioned by the spatial heterogeneity of the hydraulic conductivity which can be sharply ranged even on a small scale and within the same geological formations. In addition, the brownfields hydraulic conductivity field may be affected by the presence of concrete foundations buried in the shallow aquifers.

In general, the characterization of the hydraulic conductivity is performed by means of traditional pumping tests in which the analytical formulations of the groundwater flow equations, either in the transient or steady states, are used to interpret the piezometric responses to water extraction, in order to derive an average value of the hydraulic transmissivity (Theis 1935; Hantush 1961a, b). The permeabilities can be progressively estimated with a permeameter test carried out on soils sampled during drilling operations. However, both approaches neglect the heterogeneity of the hydraulic properties in the aquifer, which leads to an inaccurate and incomplete understanding of contaminants transport during the remediation process.

The hydraulic tomography tool appears as an interesting and relevant option to deals with the heterogeneous aquifers through a conjoint interpretation of a piezometric dataset associated with multiple pumping tests conducted successively at various wells (Yeh et al., 1996; Kitanidis, 1997, Le

51 Borgne et al. 2004; Li et al. 2008). The tomogram of the hydraulic conductivity field, provided from a
52 hydraulic tomography technique, is the result of an optimization algorithm also called "inverse
53 algorithm" in which this field was chosen thanks to its ability to match the observed drawdown data.
54 Inversion algorithms can be deterministic or stochastic. They both rely on an iterative process in
55 which the groundwater flow equations (forward problem) are solved numerically at each iteration, in
56 order to evaluate the mismatch between the observed and predicted hydraulic drawdown (Huang et
57 al. 2004). However, these inverse algorithms do not guarantee to get a unique solution for the
58 following reasons: i) the limited number of the hydraulic data to capture overall unknown parameters
59 (Zhou et al. 2016) ; ii) The strong sensitivity of the solution to the data noise (Ramos et al. 2017) ;
60 iii) The numerical uncertainty of mathematical models that cannot describe all the physical
61 mechanisms involved in the experiment, to which it adds the numerical imperfections related to the
62 numerical tool (e.g., finite difference and finite element) used to solve the groundwater equation
63 (Berg and Illman 2015; Hochstetler et al. 2016).
64 Over the last few decades, several efforts have been made to deal with the ill-posedness and the
65 uncertainties of the inverse problem via the incorporation of complementary information on the
66 unknown parameters in order to generate a realistic model (Zhou et al. 2014). This additional
67 information is referred as soft data or a priori model and can be deduced from various ways such as:
68 geological characterization (e.g, lithostratigraphic logs, grain size analyses on the soil cores) (Jardani
69 et al. 2012; Zhao et al. 2015), hydrogeological investigation (e.g, permeameter test on the soil cores,
70 tracer and slug experiments) (Sanchez-León et al. 2016) and geophysical prospections (e.g. Electrical
71 Resistivity Tomography ERT, Electromagnetic Very Low Frequency VLF, Georadar and Seismic
72 methods) (Hyndman et al. 1994; Jardani et al. 2012). Among these attempts: Soueid Ahmed et al.
73 (2015) used the geometry of the geological structures identified by geophysical tomography as a
74 priori information in the inversion of pumping test data to image hydraulic parameters. Bohling et al.

(2007) applied cross-well georadar tomography to delineate the shape of the main hydro-facies in which hydraulic conductivity values were then determined by analyzing pumping test data. GPR velocity tomograms were used to support tracer test data for the prediction of hydraulic properties (Dafflon and Barrash 2012). Jardani et al. (2013) combined the ERT, self-potential and salt concentration data acquired during a salt tracer test to map the hydraulic conductivity field. Pollock and Cirpka (2010) coupled hydrogeophysical inversion to synthetic salt tracer experiments. Doetsch et al. (2010) proposed cross-gradient joint inversion of crosshole -seismic, ERT and radar to retrieve the main geological units of a fluvial aquifer and their petrophysical parameters, as porosity. Gernez et al. (2019) linked the anisotropic patterns of the inverted electrical resistivity to the spatial distribution of the hydraulic conductivity in an alluvial aquifer.

In this paper, we apply the zonation inversion methodology to image the spatial variability of the hydraulic conductivity field. This approach consists of two steps: first, we delineate in 3D the main geological structures of a contaminated aquifer by using ERT. In the second step, we predict the hydraulic conductivity of these structures by inverting the pumping tests data recorded in 13 wells with a Markov chain Monte Carlo-based algorithm.

Description of the experimental study site

In this manuscript, a hydrodynamic characterization is performed on an experimental site located in a former refinery within a shallow alluvial aquifer contaminated by hydrocarbons. The industrial activities on the site have begun in 1929 and have been stopped in April 2013. The set up of this experimental site aims to understand the degree of heterogeneity in the soil of the former refinery and the nature of the contaminants in order to experiment various remediation protocols. For that reason, 13 piezometers were implanted on a small area (60 m x 60 m) to record the hydraulic fluctuations, and to identify the degree and type of contamination in the aquifer (Fig.1).

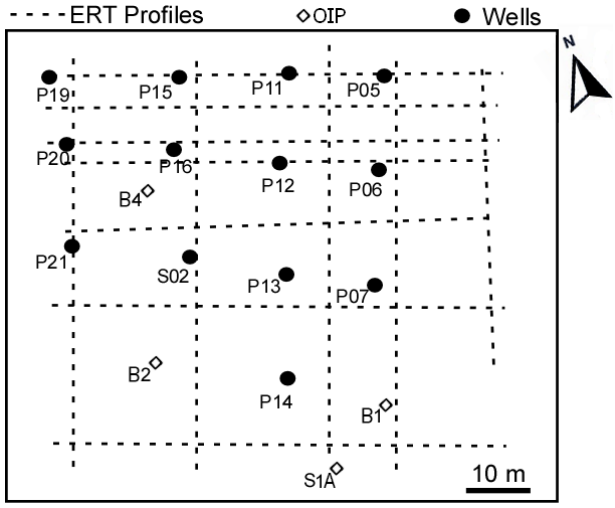

Figure 1 : Map of spatial position of ERT profiles with 2m electrodes spacing, of the wells used in the hydraulic characterization and the boreholes drilled for OIP (Optical Image Profiler) characterization

The site is mostly covered by an anthropogenic layer of gravel and in some places, of asphalt and concrete. This layer covers an alluvial formation composed mainly of fine sand (< 0.2 mm) and medium sand (< 1 mm) from 1 to 5 meters' depth, and medium (< 1 mm) to gravel sands (< 2 mm) between 5 and 8 meters depth. Preliminary geological investigations conducted on the site revealed highly heterogeneous materials constituting the aquifer. The laboratory analysis performed on three core samples indicate a quite constant porosity (from 28.9% to 24.6% between -7.2 and -10.5m), a hydraulic conductivity varying between [2.31×10^{-5} to 6.87×10^{-4} m/s] and a low quantity of clay. This alluvial terrace relies on an altered chalk formation (below -8.5 meters), and both aquifers are hydraulically connected to the Seine River; which is under tidal influence (Jardani et al., 2012). Consequently, the water table in the alluvial aquifer oscillates with time-varying amplitude.

The vertical geochemical profiles conducted on 12 wells with spacing measurement of 0.25 meters show that the water temperature is around 12 to 13°C with a vertical gradient of 0.13°C/m from 6 to 9 meters. The pH of the water is quite homogeneous between 6 and 7.5. The Redox potential fluctuates between -60 and -180 mV, which are high values. The absence of oxygen in groundwater is confirming the anaerobic conditions of the medium, which is also an index of intense process of

hydrocarbon biodegradation (Sinke et al. 1998; Abbas et al. 2018). The electrical conductivity of the water is quite homogeneous in the wells with values between 70 and 90 mS/m. All of these water measurements were realized in wells without floating LNAPL (Light Non-Aqueous Phase Liquid) layer and broadly indicate that the area is polluted with hydrocarbons and ongoing biodegradation processes that are boosted by the tide fluctuations (Mercer and Cohen 1990; Sims et al. 1993; Lee et al. 2001; Yadav and Hassanizadeh 2011).

The chromatographic analysis of LNAPL indicates a partial degradation of gasoline-diesel mixture. Moreover, the contaminant is approximately composed of 50% of light compounds (fewer than 10 carbon atoms) and the TPH (Total Petroleum Hydrocarbon) analyses confirm that the aliphatic fraction represents 80% of the total mass. Their dynamic viscosity is around 5 mm^2/s while their density is varying between 820 and 830 kg/m^3.

Geoelectrical investigations:

For the geophysical characterization, we performed 12 electrical resistivity profiles to get an idea on the main heterogeneity in the shallow aquifer. Theses 2D profiles have been made with a Syscal Pro resistivity meter and electrodes placed according to the Wenner schema with two meters as inter-electrodes distance. The stack values were fixed between 4 and 8 with a Vab maximum of 800mV and an injection time of 500 ms. The distance between the profiles is about 10 meters with 5 profiles oriented north-south and 7 profiles into east-west direction (Fig.1). The north-south profile were 46 to 64 meters long and the east-west profiles were 66 to 70 meters long for a total of 1811 quadrupoles inverted. The processing of the apparent electrical resistivity has been done in 3D using ERT-Lab64 software, developed by Multi-Phase Technologies and Geostudi Astier. This software relies on a Quasi-Newton inversion algorithm with a smoothness constraint and a forward problem solved by finite elements technique with a 0.5 m mesh for a total of 1 909 476 elements (LaBrecque et al. 1996). For the boundary conditions, we used an insulating condition at the air-ground interface

and zero potential on the rest of the boundariesThe noisy data have been processed with a robust weighting algorithm based on data variance iterative reweighting (LaBrecque et al. 1996; Morelli and LaBrecque 1996). Most of these noises are due to the bad contacts between soil and electrodes in some places covered by a 20 cm concrete layer. To improve the contact, we placed the electrodes in 30 cm hammer drilled holes.

The results of the 3D inversion of the 12 ERT profiles are obtained after 7 iterations, with a final RMSE of 0.67 Ω.m. We only present the distribution of the resistivity in the saturated and capillary zones of the alluvial layer (from 5 to 10 meters depth), which will be used in a second step as a guide to predict the hydraulic conductivity field. As shown on the figure 2 and 3, this spatial distribution of the resistivity is ranging from 5 to 180 Ω.m. On the 3D model, we can distinguish three anomalies with high relative resistivity (> 35 Ω.m) and two anomalies with quite low resistivity (< 15 Ω.m). The 2D profile presented in figure 3, highlight these heterogeneities by crossing most of the heterogeneities

If we compare the 3D model and one OIP (Optical Image Profiler) profiles, they are in the same range of value (Fig. 3). This is because the 3D model integrates larger volumes of soil while the OIP profiles are very local, with pores scale resistivity measurements. Indeed, those investigations methods are quite different. Both graphs show an increasing trend with depth from 6 to 8m and then a higher value above 8 m in link to the altered chalk. Thus, we can say that the 3D model confirms and completes the very local information from OIP profiles and water electrical conductivity of the wells. We suspect that this slight heterogeneity in electrical resistivity may be associated with the three-dimensional distribution of the flint blocks that have centimeter sizes that affects the hydrodynamic features of the aquifer. In the OIP profiles, the presence of flints is also at the origin of the increase in local resistivity (Fig. 4).

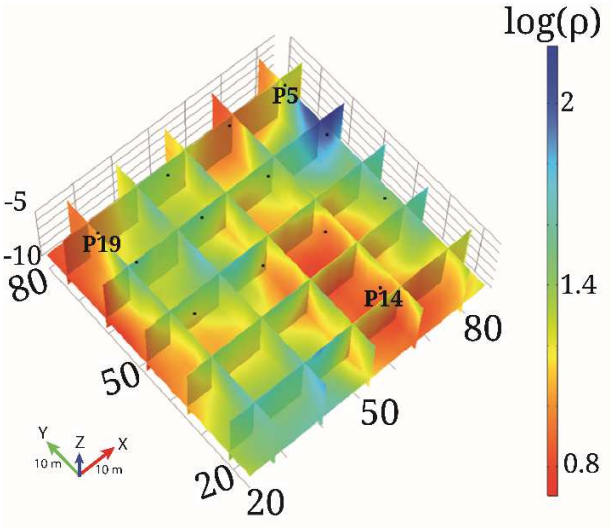

163

164 *Figure 2 : Resistivity (Ω.m) model from 3D inversion of 12 ERT profiles presented in Fig. 1*

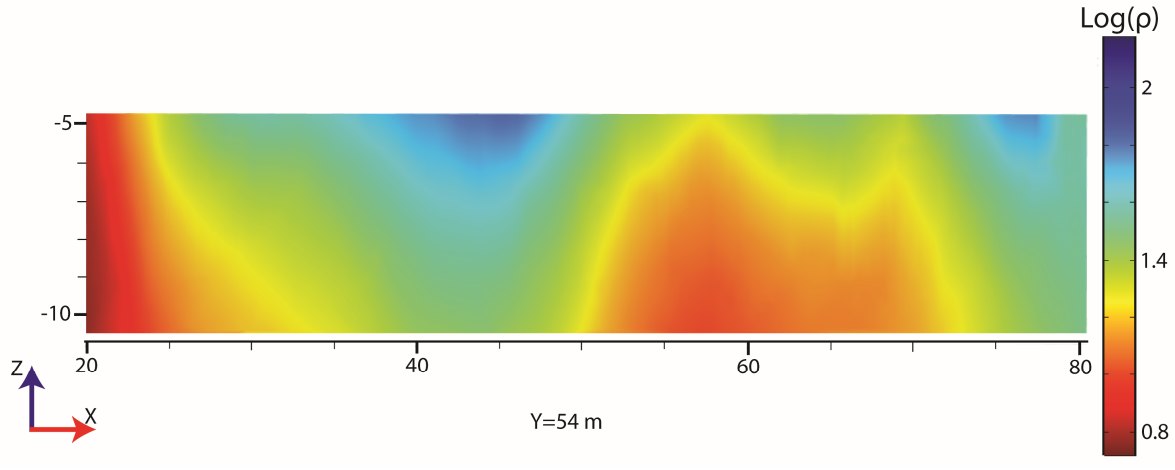

165

166 *Figure 3 : Cross-section extracted from the 3D inversion resistivity model at Y=54m.*

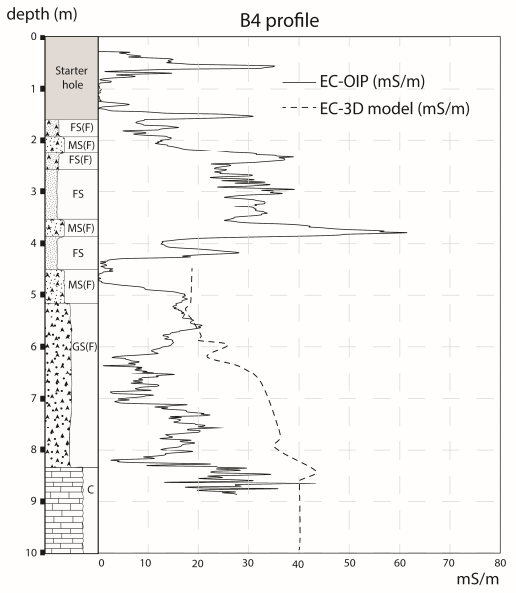

Figure 4 : Graph comparison of the 3D model of Electrical Conductivity versus OIP profile at B4 regarding with the cores granulometry description; with FS : Fine Sand ; MS : Medium Sand ; CS : Coarse Sand ; CC : cracked chalk ; (F) : Flint.

Hydrogeological investigations

We dedicate this section to the hydraulic tomography of the alluvial aquifer which is considered here as a semi-confined aquifer under tide influence. This characterization is based on a joint inversion of the hydraulic responses recorded in 13 wells during two quasi-static pumping tests conducted on the wells P16 (12 m^3/h) and P13 (11.25 m^3/h).

These hydraulic responses are also impacted with tide fluctuations, and therefore require a separation of the natural and anthropogenic responses to keep only the pumping responses for the tridimensional reconstruction of the spatial heterogeneity of the hydraulic conductivity field. The approach used for such processing is developed in the next section.

Data Processing

In this study, we will have to remove the tidal component because it has a significant impact on the hydraulic head variations in comparison to the pumping effect. In fact, daily tides have an amplitude

182 of about 20 cm while the drawdown response is under the centimeter scale. To facilitate the removal
183 of this impact, we decided to start the pumping test during the less curved part of the tide, at its mid-
184 period of 6h10, for a pumping duration of 3 hours. Such a configuration makes it easier to process
185 hydraulic data compared to a pumping at high- or low-tide momentum. The data processing relies on
186 the reconstruction of the natural tide signature by fitting the data recorded before the pumping and
187 after the recovery by predicting the coefficients of the general Fourier function with 5 terms, which
188 has following form:

189 $$F(t) = \sum_0^N (a_N \,.\cos\,(N * t * w) + \, b_N * \sin(N * t * w)\,; \qquad (1)$$

190 With N indicating the number of terms of the general function set here as N=5.

191 This equation is formulated as a sum of cosines and sines functions with 5 coefficients that will be
192 determined by fitting the hydraulic data. To illustrate the effectiveness of the technique, we applied it
193 on a theoretical case in which the groundwater flow equation was solved in a COMSOL Multiphysics
194 model with a 20 cm oscillatory tidal signal with a period of 12h20 imposed on the boundary
195 condition and a pumping test defined as a punctual source term for a duration of 3 hours. The model
196 has a homogenous hydraulic conductivity of 10^{-4} m/s and the same size as the study zone. The curve
197 fitting technique allows to distinguish the 21 mm drawdown of the hydraulic level successfully as it is
198 shown in the figure 5.a and b.

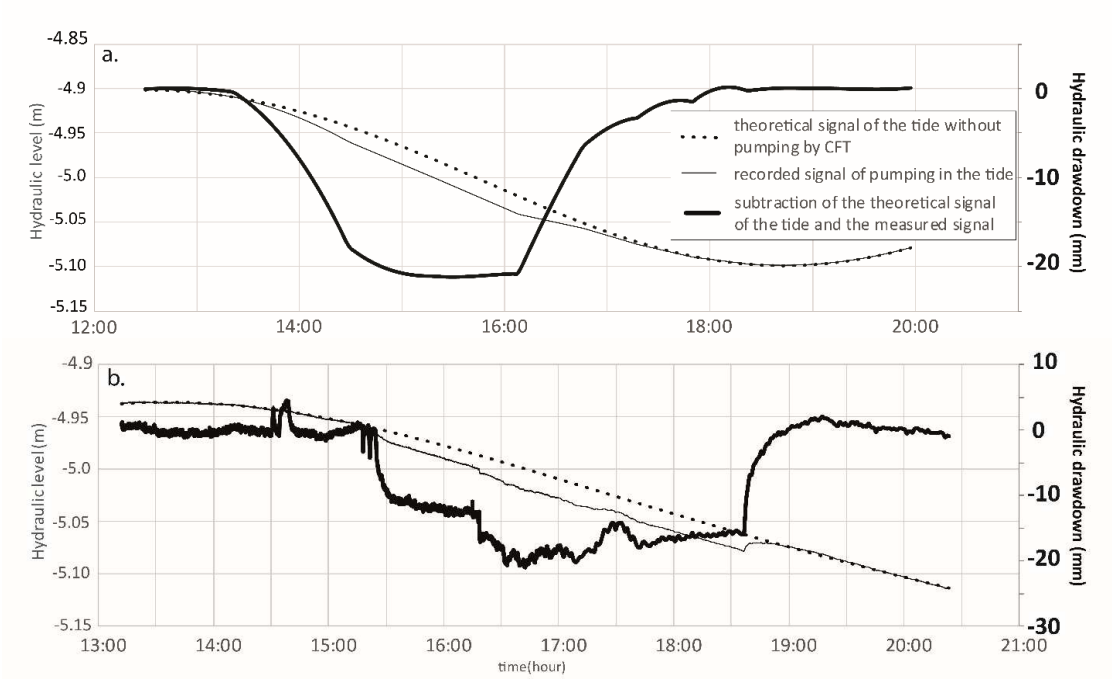

Figure 5 : graphs showing the reconstruction of the tide signal without pumping to extract the pumping drawdowns. With 4a. the numerical example and 4.b.the real hydraulic level variation.

In order to extract a steady-state drawdown value for the inversion dataset, we calculate the drawdown mean values in the last 5 minutes before cutting off the power of the pump. The inversion will be made with these mean values.

Inversion process

We devoted this section to the introduction of the inverse theory used to interpret the hydraulic data related to the pumping tests for inferring the hydraulic conductivity field in 3D. The wells are fully screened in the alluvial aquifer, thus it does not provide three-dimensional information on hydraulic head variations, especially on the Z-axis which remains an integrative data on the entire thickness of the aquifer. To fill the gap in vertical data, we used the ERT as a source of information to delineate the main heterogeneity of the field, which could correspond to variations in the hydraulic parameters. The values for the selections of the 8 electro-facies are calculated on the basis of 7 quantiles so that each electro-facies have the same size (Table 1).

Inferior value (Ω.m)	Electro-facies	Superior value (Ω.m)
	Electro-facie 1	< 8.84
8.84	Electro-facie 2	11.80
11.80	Electro-facie 3	14.92
14.92	Electro-facie 4	18.04
18.04	Electro-facie 5	21.34
21.34	Electro-facie 6	26.76
26.76	Electro-facie 7	35.84
35.84 <	Electro-facie 8	

Table 1 : upper and lower bound of the electro facies

In other words, we assume that the number and shape of electro-facies recovered in ERT remain the same in hydro-facies, so that there is a correlation between the contrast (gradient) of electrical reactivity and hydraulic conductivity. This hypothesis is based on the fact that the electrical conductivity of the water in the study site is almost homogeneous. This strategy permits to guide the inversion, to avoid the non-unicity of the solution and to reduce the number of parameters to estimate. The limited number of unknown parameters pushed us to opt for a stochastic inversion by using a MCMC algorithm. The inverse problem is formulated in a Bayesian framework in which the posteriori probability function $\pi(\mathbf{m}|\mathbf{d})$ is defined as a combination of the drawdown data of the pumping test and a priori information on the hydraulic conductivity model to be predicted during the inverse process (Tarantola 2005).

$$\pi(\mathbf{m}) \propto \mathrm{P}(\mathbf{h}_{obs}|\mathbf{m})\,\mathrm{P}_0(\mathbf{m}),$$

$$\text{With } \mathrm{P}(\mathbf{h}_{obs}|\mathbf{m}) = \frac{1}{[(2\pi)^N \det \boldsymbol{\Gamma}_h]^{1/2}} \exp\left[-\frac{1}{2}\left(f(\mathbf{m})-\mathbf{h}_{obs}\right)^{\mathrm{T}} \boldsymbol{\Gamma}_h^{-1}\left(f(\mathbf{m})-\mathbf{h}_{obs}\right)\right],$$

227 $$P_0(\mathbf{m}) = \frac{1}{[(2\pi)^M \det \boldsymbol{\Gamma}_\mathbf{m}]^{1/2}} \exp\left[-\frac{1}{2}\left(\mathbf{m}-\mathbf{m}_{\text{prior}}\right)^T \boldsymbol{\Gamma}_m^{-1}\left(\mathbf{m}-\mathbf{m}_{\text{prior}}\right)\right], \quad (2)$$

228 where $P_0(\mathbf{m})$ denotes the prior probability, function used as a complementary information to
229 constrain the parameter $\mathbf{m}$ in the prediction process of the model. $\boldsymbol{\Gamma}_m$is the covariance matrix
230 representing the degrees of confidence to the prior values $\mathbf{m}_{\text{prior}}$. $P(\mathbf{h}_{obs}|\mathbf{m})$ denotes the likelihood
231 function in which a forward operator $f(\mathbf{m})$ is solved numerically to compute the effectiveness of the
232 proposed model $\mathbf{m}$ to fit the hydraulic data $\mathbf{h}_{obs}$. $\boldsymbol{\Gamma}_h$ is a diagonal covariance matrix to include
233 uncertainties on the observed data. This inversion operator is based on a numerical resolution of the
234 diffusion equation with Darcy groundwater flow in porous media.

235 $$\begin{cases} \nabla.(-10^{-m}.\nabla h) = Q\,, & \text{in 3D} \\ h = 0\ m, & \text{at } \Gamma_D \end{cases} \quad (3)$$

236 Where h denotes the hydraulic head (in meter), Q is the hydraulic flux (m^3/s) and $\mathbf{m}$ is the vector
237 that contains the logarithms of the hydraulic conductivity K (in m/s).
238 We solve the diffusion equation on a pyramidal finite element mesh with COMSOL Multiphysics.
239 The meshing is defined as extremely fine with an automatic refinement around the boreholes.
240 Dirichlet boundary conditions were imposed on the boundaries, which were placed at 500 m from
241 the investigated zone. The investigation zone is 60 by 60 meters with the hydraulic conductivity of
242 the buffer fixed to $10^{-2.1}$ m/s.
243 The stochastic inversion was led with a large constraint on the hydraulic conductivity in which the
244 interval of sampling was fixed between 10^{-8} and 1. To seek the best model that can reconstruct the
245 hydraulic data and satisfy the constraints imposed by the prior information, we applied a stochastic
246 approach which is based on a MCMC algorithm. This algorithm consists in a generation of an
247 important number of random models using a proposal function. It then tests their efficiency in terms

of data-matching and toward the prior models by computing the posterior probability function. The models tested with high probabilities are selected, otherwise they are rejected. The implementation of such approach does not imply any derivative computation of the forward problem, as it is the case in deterministic algorithms, which facilitates the implementation of such algorithm. However, their efficiency depends on the choice of the proposal density function that controls the random walk from one last selected model to the generation of another new one. In this paper, we used Adaptive Metropolis (AM) algorithm in which the covariance of Gaussian proposal function is iteratively adapted from the previous models in order to improve the strategy of the sampling as following (Haario et al. 2001) :

$$C_i = S_d Cov(X_0, X_1, \dots, X_{i-1}) + S_d \varepsilon I \quad (4)$$

Where $S_d = (2.4)^2 / d$, is a scaling coefficient with d the size of the unknown parameter to estimate, ε is a small positive number and I is the identity matrix. The model proposed with the proposal function will be accepted or rejected according to this following probability:

$$\alpha(m_{i-1}, m_p) = min\left(1, \frac{\pi(m_p)}{\pi(m_{i-1})}\right) \quad (5)$$

Where $\pi(x)$ is the unscaled density, m_p is the tested candidate when the *i-1* previous candidate has already been tested. In the end, these acceptance criteria guarantee the selection of models that present high quality in the fitting of the piezometric data. In our case, 10 000 iterations were carried out and the inverse result is the mean of the last 25 selected models.

Results

The result is presented as a 3D model in terms of logarithm values of hydraulic conductivity (K in m/s in Fig. 6). The inversion has been made on the mean drawdown value determined during the last 5 minutes of pumping. The means, minimum and maximum value of these last 5 minutes of pumping are shown on the figure 7.

271 The Root Mean Square Error (RMSE) of the inversion between all the measured and simulated
272 drawdown is 5.23 mm. The coefficient of determination is almost perfect, as the weight of the
273 pumping well drawdown is much more important compared to the small drawdown in the
274 observation wells, and the slope of the linear regression is near one (a=0.9995). These values have a
275 weaker fit if we focused on the observation wells drawdowns, but it can be related to the greater
276 uncertainty about the actual value of the smallest drawdown. Indeed, if we only focused on the
277 observation wells drawdown, the R^2 is about 0.73 with a slope near 0.9 (a=0.908). The RSME
278 becomes a bit bigger: 5.37 mm.

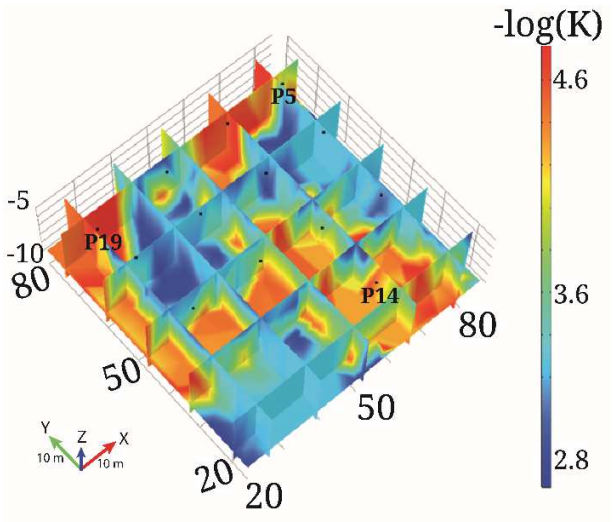

279

280 *Figure 6 : Hydraulic conductivity (m/s) model after the stochastic inversion to reproduce the pumping drawdown*

281 The small drawdowns are related to the low hydraulic connectivity, the large distance between
282 observation and pumped wells, and the possibility that the pumped water is mainly coming from the
283 underlying aquifer in the altered chalk.

Electro-facies	- Log(K)
Electro-facie 1	4.450
Electro-facie 2	4.710
Electro-facie 3	4.762

Electro-facie 4	3.603
Electro-facie 5	2.684
Electro-facie 6	3.095
Electro-facie 7	3.278
Electro-facie 8	3.269

Table 2: hydraulic conductivities of the 8 electro-facies

The 3D model reveals a smooth spatial heterogeneity with a variation of only 2 orders of magnitude. The inverted values of hydraulic conductivity range (between 10^{-3} and 10^{-5} m/s as detailed in the table 2) are realist and in agreement with the laboratory results range (between $4.76.10^{-4}$ to $2.31.10^{-5}$ m/s). There is an order of magnitude of difference between the lab result and our model. This can be linked to the size of the lab sample which tends to decrease the measured value (Geotechnical Frontiers et al. 2017).Overall, the aquifer can be considered as a permeable formation linked to the presence of the gravels and flint blocks that have been revealed by their resistive signature in the electrical resistivity survey. As it is confirmed by the results of the comparisons between the high electro-facies (5 to 8) that have relative higher hydraulic conductivities (see table 2).

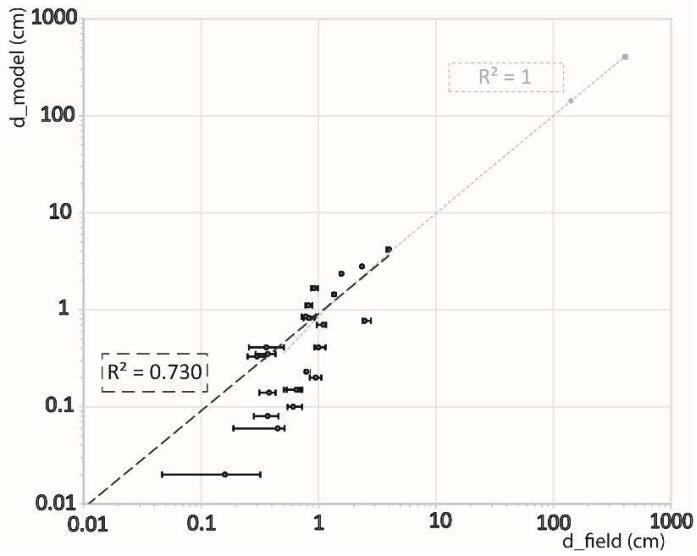

Figure 7 : graph of measured (d_field) versus simulated (d_model) drawdowns with the error bar representing the max and min drawdown observed during the last 5 minutes of pumping.

In order to discuss further 3D hydraulic model obtained by stochastic inversion from the 3D electrical resistivity model, it was decided to perform trials of stepwise pumping in different wells in the study area. These pumping have been realized with an Electric Variable speed drive and a small pump. This device allows for stepwise pumping by varying the frequency (i.e. the flow rate) of the pump from 0.6 to 6.1 m^3/h. Every pumping lasted about 30 minutes and 2 to 4 flow rates were tested depending on the observed drawdown in the pumped well.

The drawdown data have been treated as presented in data processing section in order to subtract the tide signal and then implemented in a software to treat stepwise pumping: *OUAIP*, created by the French institution *"Bureau des Ressources Géologiques et Minières (BRGM)"*. We use the Theis function to simulate the pumping and the software provides an estimation of the transmissivity T (m^2/s) and Storativity required to fit the stepwise pumping drawdowns. There is an adjustment coefficient "E" to validate the fitting (the closest to 1, the better), also called the Nash coefficient. This Nash coefficient has values above 0.9 in our cases. To be able to compare the result, we have made the

integration of the different hydraulic conductivity K of the 3D model on the thickness of the aquifer to get a transmissivity value at the localization of the different wells.

Wells tested	-log T model	-log T classic
P6	2.57	2.93
P11	4.03	3.01
P14	3.75	3.70
B4	2.53	2.41

Table 3 : comparison of classic versus 3D model values of – log Transmissivity

If the P11 transmissivity from the pumping is one order of magnitude smaller compared to the value found in the model, the three other values are convergent and validate the 3D stochastic inversion of the hydraulic model.

Discussion and conclusion

The use of electrical resistivity data to characterize the spatial heterogeneities appeared as particularly suitable for determining the properties of the medium studied in our application case and allowed for an easier and more complete identification of its hydraulic properties. We tried to use this link to inverse hydraulic data on the basis of electrical resistivity heterogeneities. This does not mean that there is a direct relationship defined in this article between electrical resistivity and hydraulic conductivity (Mazac et al. 1990; Borner et al. 1996; Attwa and Ali 2018; Maurya et al. 2018; Weller and Slater 2019).

The advantages of the geophysics are well known. The 3D data of electrical resistivity provide a good and quick characterization of the heterogeneities of lithology in the aquifer. Indeed, the ERT is a useful non-invasive method for characterising the sub-surface soils in terms of their electrical properties. Electrical resistivity typically correlates with variations in lithology, water saturation,

340 temperature, fluid conductivity and porosity. As we worked with the electrical variations in the
341 saturated zone, the variations observed in the electrical model only reflect the variations in lithology
342 and particularly the presence of the flint blocs in the discontinuous ways in the aquifer that have a
343 resistive signature in 3D ERT model. The use of quasi-static pumping data permitted to transform
344 these electrical conductivities into hydraulic conductivity while maintaining the knowledge of the
345 heterogeneities. Incorporating geophysics information also allowed to reduce the number of
346 hydraulic parameters to be inverted. Instead of working with a regular grid of unknown parameters
347 in the model, we only worked with 8 uniform zones. Naturally, the more zones we would define for
348 the inversion in the model, the longer the inversion would become without necessarily improving the
349 result. Our 3D models integrating geophysical information made it possible to approach more
350 faithfully the vertical heterogeneities not displayable in 2 dimensions. Indeed, the classic pumping
351 tests data we used are integrative along the depths of the aquifers in which one pumps. An
352 alternative solution would be to use flowmeters in order to characterize the recharge zones according
353 to lithology (Kabala 1994 ; Paillet and Morin 1997 ; Li et al. 2008). In addition, pneumatic packers
354 can be used to isolate a pumping over a fixed thickness of the aquifer to characterize a more
355 specified lithology of the aquifer (Levy et al. 1993 ; Bohling et al. 2007 ; Cardiff et al. 2013 ; Paradis
356 et al. 2016). But this would increase the number of pumping, and therefore the amount of water
357 pumped to be treated in the event of a contaminated aquifer. However, a supplementary amount of
358 data to be inverted would also allow for a better characterization of the aquifer.
359 Another problematic encountered in our field with hydraulic data was that the natural tide signals did
360 not simplify the acquisition of the drawdowns in response to the pumping tests. Besides, the tidal
361 coefficient influenced the drawdowns. In fact, the underlying altered chalk aquifer is the most direct
362 link between the Seine river and the study area and the variations of exchanges between these two
363 aquifer units in high tide coefficients or low tide coefficients affect the recharge rate and therefore

364 the water table level in the aquifer while pumping. Performing a cross oscillatory pumping appears as
365 an interesting possible alternative as it makes it possible to extract the oscillatory variations data with
366 a Fourier Transform (Bakhos et al. 2014; Fischer et al. 2018) according to their known pumping-rate
367 frequency of oscillation.
368 Overall, we observed in this aquifer a high permeable structure with the hydraulic conductivity
369 ranging from the [$10^{-2.8}$, $10^{-4.6}$] and these slight variations seem dependent on the presence or absence
370 of the flint blocs that heightened the transmissivity. The presence of the flints is electrically identified
371 by the resistive values in the electrical resistivity model. The reconstruction is sufficient to determine
372 the relative low and high hydraulic conductivity zones to better understand the aquifer behavior.

373 ## Acknowledgments

374 We gratefully thank the Normandy Region and ADEME for their financial support of this work and
375 the reviewers for their pertinent suggestions.

References:

Abbas M, Jardani A, Machour N, Dupont J-P (2018) Geophysical and geochemical characterisation of a site impacted by hydrocarbon contamination undergoing biodegradation. Near Surface Geophysics 16:176–192. https://doi.org/10.3997/1873-0604.2017061

Attwa M, Ali H (2018) Resistivity Characterization of Aquifer in Coastal Semi arid Areas: An Approach for Hydrogeological Evaluation. In: Groundwater in the Nile Delta. Springer International Publishing, Cham, pp 213–233

Bakhos T, Cardiff M, Barrash W, Kitanidis PK (2014) Data processing for oscillatory pumping tests. Journal of Hydrology 511:310–319. https://doi.org/10.1016/j.jhydrol.2014.01.007

Berg SJ, Illman WA (2015) Comparison of Hydraulic Tomography with Traditional Methods at a Highly Heterogeneous Site. Groundwater 53:71–89. https://doi.org/10.1111/gwat.12159

Bohling GC, Butler JJ, Zhan X, Knoll MD (2007) A field assessment of the value of steady shape hydraulic tomography for characterization of aquifer heterogeneities: A FIELD ASSESSMENT OF HYDRAULIC TOMOGRAPHY. Water Resour Res 43:. https://doi.org/10.1029/2006WR004932

Borner FD, Schopper JR, Weller A (1996) Evaluation of transport and storage properties in the soil and groundwater zone from induced polarization measurements. Geophys Prospect 44:583–601. https://doi.org/10.1111/j.1365-2478.1996.tb00167.x

Cardiff M, Barrash W, Kitanidis PK (2013) Hydraulic conductivity imaging from 3-D transient hydraulic tomography at several pumping/observation densities: Hydraulic Tomography Imaging Resolution. Water Resour Res 49:7311–7326. https://doi.org/10.1002/wrcr.20519

Dafflon B, Barrash W (2012) Three-dimensional stochastic estimation of porosity distribution: Benefits of using ground-penetrating radar velocity tomograms in simulated-annealing-based or Bayesian sequential simulation approaches: 3-D STOCHASTIC ESTIMATION OF POROSITY. Water Resour Res 48:. https://doi.org/10.1029/2011WR010916

Doetsch J, Linde N, Coscia I, et al (2010) Zonation for 3D aquifer characterization based on joint inversions of multimethod crosshole geophysical data. GEOPHYSICS 75:G53–G64. https://doi.org/10.1190/1.3496476

Fischer P, Jardani A, Jourde H, et al (2018) Harmonic pumping tomography applied to image the hydraulic properties and interpret the connectivity of a karstic and fractured aquifer (Lez aquifer, France). Advances in Water Resources 119:227–244. https://doi.org/10.1016/j.advwatres.2018.07.002

Geotechnical Frontiers, Brandon TL, Valentine RJ, et al (2017) Geotechnical Frontiers 2017. selected papers from sessions of Geotechnical Frontiers 2017, March 12-15, 2017, Orlando, Florida

Gernez S, Bouchedda A, Gloaguen E, Paradis D (2019) Comparison Between Hydraulic Conductivity Anisotropy and Electrical Resistivity Anisotropy From Tomography Inverse Modeling. Front Environ Sci 7:67. https://doi.org/10.3389/fenvs.2019.00067

412 Haario H, Saksman E, Tamminen J (2001) An adaptive Metropolis algorithm. Bernoulli 223–242

413 Hantush MS (1961a) Drawdown Around a Partially Penetrating Well. Journal of the Hydraulics Division
414 83–98

415 Hantush MS (1961b) Aquifer Tests on Partially Penetrating Wells. Journal of the Hydraulics Division 171–
416 195

417 Hochstetler DL, Barrash W, Leven C, et al (2016) Hydraulic Tomography: Continuity and Discontinuity of
418 High- *K* and Low- *K* Zones: D. L. Hochstetler. Groundwater 54:171–185.
419 https://doi.org/10.1111/gwat.12344

420 Hohmann, G. W., 1988, Numerical modeling for electromagnetic methods in geophysics, in Nabighian,
421 M. N., Eds., Electromagnetic methods in geophysics, 1: Society of Exploration Geophysicists, Invest. in
422 Geophys., no. 3, 313-363.

423 Huang H, Hu BX, Wen X-H, Shirley C (2004) Stochastic inverse mapping of hydraulic conductivity and
424 sorption partitioning coefficient fields conditioning on nonreactive and reactive tracer test data:
425 INVERSE MAPPING CONDITIONING ON TRACER DATA. Water Resour Res 40:.
426 https://doi.org/10.1029/2003WR002253

427 Hyndman DW, Harris JM, Gorelick SM (1994) Coupled seismic and tracer test inversion for aquifer
428 property characterization. Water Resour Res 30:1965–1977. https://doi.org/10.1029/94WR00950

429 Jardani A, Dupont JP, Revil A, et al (2012) Geostatistical inverse modeling of the transmissivity field of a
430 heterogeneous alluvial aquifer under tidal influence. Journal of Hydrology 472–473:287–300.
431 https://doi.org/10.1016/j.jhydrol.2012.09.031

432 Jardani A, Revil A, Dupont JP (2013) Stochastic joint inversion of hydrogeophysical data for salt tracer test
433 monitoring and hydraulic conductivity imaging. Advances in Water Resources 52:62–77.
434 https://doi.org/10.1016/j.advwatres.2012.08.005

435 Kabala ZJ (1994) Measuring distributions of hydraulic conductivity and specific storativity by the double
436 flowmeter test. Water Resour Res 30:685–690. https://doi.org/10.1029/93WR03104

437 P. K. Kitanidis, (1997) Introduction to Geostatistics: Applications in Hydrogeology, University Press,
438 Cambridge, 1997, pp. 86-95.
439 LaBrecque DJ, Miletto M, Daily W, et al (1996) The effects of noise on Occam's inversion of resistivity
440 tomography data. GEOPHYSICS 61:538–548. https://doi.org/10.1190/1.1443980

441 Le Borgne T, Bour O, de Dreuzy JR, et al (2004) Equivalent mean flow models for fractured aquifers:
442 Insights from a pumping tests scaling interpretation : equivalent mean flow models. Water Resour Res
443 40:. https://doi.org/10.1029/2003WR002436

444 Lee C-H, Lee J-Y, Cheon J-Y, Lee K-K (2001) Attenuation of Petroleum Hydrocarbons in Smear Zones: A
445 Case Study. J Environ Eng 127:639–647. https://doi.org/10.1061/(ASCE)0733-9372(2001)127:7(639)

446 Levy BS, Pannell LJ, Dadoly JP (1993) A pressure-packer system for conducting rising head tests in water
447 table wells. Journal of Hydrology 148:189–202. https://doi.org/10.1016/0022-1694(93)90259-C

448 Li W, Englert A, Cirpka OA, Vereecken H (2008) Three-Dimensional Geostatistical Inversion of Flowmeter
449 and Pumping Test Data. Ground Water 46:193–201. https://doi.org/10.1111/j.1745-
450 6584.2007.00419.x

451 Maurya PK, Balbarini N, Møller I, et al (2018) Subsurface imaging of water electrical conductivity,
452 hydraulic permeability and lithology at contaminated sites by induced polarization. Geophysical
453 Journal International 213:770–785. https://doi.org/10.1093/gji/ggy018

454 Mazac O, Císlerová M, Kelly WE, et al (1990) 14. Determination of Hydraulic Conductivities by Surface
455 Geoelectrical Methods. In: Geotechnical and Environmental Geophysics: Volume II, Environmental
456 and Groundwater. Society of Exploration Geophysicists, pp 125–132

457 Mercer JW, Cohen RM (1990) A review of immiscible fluids in the subsurface: Properties, models,
458 characterization and remediation. Journal of Contaminant Hydrology 6:107–163.
459 https://doi.org/10.1016/0169-7722(90)90043-G

460 Morelli G, LaBrecque D (1996) Advances in ERT inverse modeling. European Journal of Environmental
461 and Engineering Geophysics 1:171–186

462 Ossai IC, Ahmed A, Hassan A, Hamid FS (2020) Remediation of soil and water contaminated with
463 petroleum hydrocarbon: A review. Environmental Technology & Innovation 17:100526.
464 https://doi.org/10.1016/j.eti.2019.100526

465 Paillet FL, Morin RH (1997) Hydraulic tomography in fractured bedrock aquifers using high-resolution
466 borehole flowmeter measurements. Geological Society, London, Engineering Geology Special
467 Publications 12:267–272. https://doi.org/10.1144/GSL.ENG.1997.012.01.23

468 Paradis D, Gloaguen E, Lefebvre R, Giroux B (2016) A field proof-of-concept of tomographic slug tests in
469 an anisotropic littoral aquifer. Journal of Hydrology 536:61–73.
470 https://doi.org/10.1016/j.jhydrol.2016.02.041

471 Pollock D, Cirpka OA (2010) Fully coupled hydrogeophysical inversion of synthetic salt tracer
472 experiments: fully coupled hydrogeophysical inversion. Water Resour Res 46:.
473 https://doi.org/10.1029/2009WR008575

474 Ramos G, Carrera J, Gómez S, et al (2017) A stable computation of log-derivatives from noisy drawdown
475 data: computation of moisy log-derivatives. Water Resour Res 53:7904–7916.
476 https://doi.org/10.1002/2017WR020811

477 Sanchez-León E, Leven C, Haslauer CP, Cirpka OA (2016) Combining 3D Hydraulic Tomography with
478 Tracer Tests for Improved Transport Characterization: E. Sanchez-León et al. Groundwater XX, no. X:
479 XX-XX. Groundwater 54:498–507. https://doi.org/10.1111/gwat.12381

480 Sims JL, Sims RC, Dupont RR, et al (1993) In situ bioremediation of contaminated unsaturated subsurface
481 soils

482 Sinke AJC, Dury O, Zobrist J (1998) Effects of a fluctuating water table: column study on redox dynamics
483 and fate of some organic pollutants. Journal of Contaminant Hydrology 33:231–246.
484 https://doi.org/10.1016/S0169-7722(98)00072-2

485 Soueid Ahmed A, Zhou J, Jardani A, et al (2015) Image-guided inversion in steady-state hydraulic
486 tomography. Advances in Water Resources 82:83–97.
487 https://doi.org/10.1016/j.advwatres.2015.04.001

488 Tarantola A (2005) Inverse Problem Theory and Methods for Model Parameter Estimation. Society for
489 Industrial and Applied Mathematics

490 Theis CV (1935) The relation between the lowering of the Piezometric surface and the rate and duration
491 of discharge of a well using ground-water storage. Trans AGU 16:519.
492 https://doi.org/10.1029/TR016i002p00519

493 Weller A, Slater L (2019) Permeability estimation from induced polarization: an evaluation of geophysical
494 length scales using an effective hydraulic radius concept. Near Surface Geophysics 17:581–594.
495 https://doi.org/10.1002/nsg.12071

496 Yadav BK, Hassanizadeh SM (2011) An Overview of Biodegradation of LNAPLs in Coastal (Semi)-arid
497 Environment. Water Air Soil Pollut 220:225–239. https://doi.org/10.1007/s11270-011-0749-1

498 Yeh, T.-C. J., Jin, M. &Hanna, S. (1996) An iterative stochastic inverse method: conditional effective
499 transmissivity and hydraulic head fields. Wat. Resour. Res. 32(1), 85-92

500 Yeung AT (2010) Remediation Technologies for Contaminated Sites. In: Chen Y, Zhan L, Tang X (eds)
501 Advances in Environmental Geotechnics. Springer Berlin Heidelberg, Berlin, Heidelberg, pp 328–369

502 Zhang S, Mao G, Crittenden J, et al (2017) Groundwater remediation from the past to the future: A
503 bibliometric analysis. Water Research 119:114–125. https://doi.org/10.1016/j.watres.2017.01.029

504 Zhao Z, Illman WA, Yeh T-CJ, et al (2015) Validation of hydraulic tomography in an unconfined aquifer: A
505 controlled sandbox study: hydraulic tomography in an unconfined aquifer. Water Resour Res
506 51:4137–4155. https://doi.org/10.1002/2015WR016910

507 Zhou H, Gómez-Hernández JJ, Li L (2014) Inverse methods in hydrogeology: Evolution and recent trends.
508 Advances in Water Resources 63:22–37. https://doi.org/10.1016/j.advwatres.2013.10.014

509 Zhou Y, Lim D, Cupola F, Cardiff M (2016) Aquifer imaging with pressure waves-Evaluation of low-impact
510 characterization through sandbox experiments: AQUIFER IMAGING WITH PRESSURE WAVES. Water
511 Resources Researches 52:2141–2156. https://doi.org/10.1002/2015WR017751

512